Journal of Photochemistry and Photobiology A: Chemistry 199 (2008) 136–143

Contents lists available at ScienceDirect

Journal of Photochemistry and Photobiology A: Chemistry

journal homepage: www.elsevier.com/locate/jphotochem

Visible-light driven TiO_2 photocatalysts from Ti-oxychloride precursors

P. Sampedro [a], G. Colón [b,*], M. Fernández-García [a,**]

[a] Instituto de Catálisis y Petroleoquímica, CSIC, Campus Cantoblanco, 28049 Madrid, Spain
[b] Instituto de Ciencia de Materiales de Sevilla, Centro Mixto CSIC-Universidad de Sevilla, C/Américo Vespucio, 49, 41092 Sevilla, Spain

ARTICLE INFO

Article history:
Received 27 February 2008
Received in revised form 5 May 2008
Accepted 7 May 2008
Available online 15 May 2008

Keywords:
Photocatalysis
Calcination
Hydrothermal
TiO_2
Anatase
N-doping and impurity
Visible light
Sunlight
Pollutant elimination and degradation

ABSTRACT

Series of nanosized anion-containing TiO_2-base materials with anatase-type structure were synthesized from N, Cl-containing precursors using two preparation methods, calcination and hydrotreatment. Samples were conditioned by a final calcination step in order to get free of surface anion impurities and their structural properties characterized by a combined X-ray diffraction (XRD), scanning (SEM) and transmission (TEM) microscopy, X-ray energy dispersive (XEDS), X-ray photoelectron (XPS), and diffuse reflectance infrared Fourier transform (DRIFTS) study. The structural characterization was used to interpret the UV–vis spectra. The resulting joint information allowed the rationalization of the photocatalytic activity observed for the visible-light-assisted liquid-phase degradation of phenol. We founded that maximization of photoactivity is not related with the net absorption power of our systems in the visible range but mostly driven by a combination of two characteristics; the adequate morphological properties and the presence of negatively charged N-containing species.

1. Introduction

Photocatalytic destruction of organic pollutants in the presence of TiO_2 appears as a viable decontamination process of widespread application, no matter the state (gas or liquid) or chemical nature of the process target [1,2]. TiO_2-anatase is a n-type semiconductor having a wide bandgap (3.0–3.4 eV depending on primary particle size and other properties) which necessitates UV light to create energy-rich electron–hole pairs upon absorption. All TiO_2-based technological applications aiming to use solar light as the energy source are thus limited and typically would need to optimize the handling of visible-light photons by the catalytic solid. This appears of prime importance and, furthermore, corresponds to an appealing challenge for the future generation of photocatalytic materials [3–6].

The pioneering work of Asahi et al. [7] highlighted the possibility of doping the TiO_2-anatase structure with anions to yield new, high-performance visible-light driven photocatalysts. After this report the use of N^{3-}, C^{4-}, S^{4-} or halides (F^-, Cl^-, Br^-, I^-), as doping agents has been subjected to intense research and summarized in several review articles [3,5,8,9]. Recently, several ways have been explored in order to improve and maximize the photo-activity of anion-doped titania systems and, among them, a fruitful one departs from the combination of nitrogen and halides. Reports concerning the use of N/F [10,11] and N/I [12] showed notable improvements over N-alone TiO_2-doped materials. Although essentially an open question, the improvement may come from the correct combination of the well-known N-impurity electronic levels located near the conduction band [13,14], either with the halide-modified conduction band [12] or with new color (F/F^+) centers [11]. In both cases, the visible-light absorption power is neatly enhanced. Additionally, in certain N-containing systems, the presence of a substantial amount of defects associated with the titania anion sublattice but with no direct correlation with the N-impurities creates empty electronic levels at about 2.0–2.5 eV from the upper part of the valence band [15,16], which may be strongly influenced by the presence of color centers detected in halide-containing materials. Apart from electronic matters, another point of importance in fluoride-doped systems concerns the surface acidity generated by the presence of surface anions [11].

In this work, we try to explore a novel N/Cl combination and develop a preparation process based on the precipitation of ammonium Ti-oxychlorides as initial solid precursors. This would allow to have a large doping N concentration in the precursor as well

* Corresponding author.
** Corresponding author. Tel.: +34 91 585 4939; fax: +34 91 585 4760.
E-mail addresses: gcolon@icmse.csic.es (G. Colón), mfg@icp.csic.es (M. Fernández-García).

1010-6030/$ – see front matter © 2008 Elsevier B.V. All rights reserved.
doi:10.1016/j.jphotochem.2008.05.008

as a variable Ti:Cl atomic ratio and to study the influence of these two parameters in the final structural and morphological features of the TiO_2 phase after calcination/hydrotreatment. Our main aim is to analyze the nature and amount of the impurity species and to correlate these with the photo-activity of the titania solids in the liquid-phase elimination of phenol. Materials are subjected to calcinations and/or hydrotreatment but a final, fixed calcination step was always applied in order to ensure the surface chemical uniformity of the samples. This is important as some doping surface species as chloride may change acid/base properties of the solid, may be leached from the surface during reaction (introducing uncertainties), and may drive to a lack of long-term stability. As detailed below, our systems will be essentially free of N, Cl surface adsorbed species which may be interfering in the interpretation of the results. The task to identify N, Cl-containing species is not easy as, for example, N–Ti–O, Ti–N–O (oxynitride), NO^+, N^-, N^{3-}, NH^-, or NH_x have been detected in the case of nitrogen-doped samples [3,5,7,8,13–15]. To this end, in this report we will describe the preparation and characterization of titania solids using a combination of XPS, Infrared (DRIFTS), SEM, TEM and XEDS. The joint analysis of the structural characterization and the electronic implications derived by UV–vis spectroscopy would be used to interpret photo-activity, highlighting key properties responsible for the enhancement of titania photo-activity in anion-doped TiO_2-based photocatalysts.

2. Experimental

In order to vary the Ti:Cl ratio of our precursor solids within the 1:1 to 1:6 ratio, we prepared the corresponding Ti-isopropoxide:HCl mixtures in isopropanol. The so-formed Ti:Cl complexes were stirred in a water/isopropanol (1:10) mixture for 4 h and subsequently precipitated with an ammonia solution corresponding to a NH_3:Ti ratio of 3. Solids were filtered and washed with distilled water, dried at 383 K and finally subjected to hydro- and/or calcinations treatments. Calcined samples were subjected to a heating ramp of 2 K/min up to 723 K in a (20%) O_2/N_2 atmosphere. The hydrotreated set of samples were obtained by placing the solid precursor together with 1 M NH_3 solution (30 ml/g of precursor) in a Teflon-lined reactor at 120 °C for a period between 3 and 24 h. These materials were subsequently filtered and dried at 383 K and calcined at 723 K following the above-mentioned recipe. A blank is obtained using a similar procedure but without HCl and ammonia in the preparation and precipitation steps of the precursor solid. Samples are described by an initial set of letters (B blank; TC1 and TC6 for samples prepared with Ti:Cl ratios of, respectively, 1:1 and 1:6) followed by another set describing the treatment (no letter for calcinations; HT for hydrotreatment). Table 1 summarizes the sample labels and corresponding treatment details, and gives their main physico-chemical characteristics.

X-ray diffraction (XRD) patterns were obtained using a Siemens D-501 diffractometer with Ni filter and graphite monochromator. The X-ray source was Cu Kα radiation. From the line broadening of corresponding X-ray diffraction peaks, according to the Scherrer equation (peaks were fitted by using a Voigt function).

$$D = \frac{\lambda 180}{\pi \cos\theta L}$$

where L is the line width at medium height, λ the wavelength of the X-ray radiation 0.15406 nm and θ is the diffracting angle.

XPS data were recorded on 4 mm × 4 mm pellets, 0.5-mm thick, prepared by gently pressing the powdered materials which were outgassed in the prechamber of the instrument at 150 °C up to a pressure below 2×10^{-8} Torr to remove chemisorbed water from their surfaces. The Leibold-Heraeus LHS10 spectrometer main chamber, working at a pressure < 2×10^{-9} Torr, was equipped with an EA-200 MCD hemispherical electron analyzer with a dual X-ray source working with Al Kα ($h\nu$ = 1486.6 eV) at 120 W, 30 mA. C 1s was used as energy reference (284.6 eV).

Table 1
Main synthesis details and physico-chemical characteristics of samples

Sample	S_{BET} ($m^2\,g^{-1}$)	Particle size (nm)
B	107.4	10.4
B-HT3	117.9	10.7
B-2HT3	101.2	13.1
B-HT6	143.1	11.7
B-HT24	120.1	12.3
TC1	104.9	11.9
TC1-HT3	123.9	11.8
TC1-2HT3	135.3	11.5
TC1-HT6	94.2	14.7
TC1-HT24	78.6	16.0
TC6	110.0	12.0
TC6-HT3	153.3	10.7
TC6-2HT3	141.4	10.8
TC6-HT6	93.2	14.9
TC6-HT24	90.0	15.3

Diffuse reflectance infrared spectra (DRIFTS) were taken in Bruker Equinox 55 FTIR spectrometer fitted with an MCT detector. The spectra consisted of 400 accumulations with a total of 5 min acquisition time, using a 4-cm^{-1} resolution. UV–vis diffuse reflectance spectroscopy experiments were performed with a Shimadzu UV2100 apparatus with a nominal resolution of ca. 5 nm using $BaSO_4$ as reference.

Scanning electron microscopy (SEM) pictures were taken on a JEOL JSM-5400 scanning electron microscope equipped with an energy dispersive X-rays analysis (XEDS) Link system for qualitative chemical analysis. Fractured samples were deposited on copper supports and covered by a thin film of gold.

Selected samples were also studied by transmission electron microscopy (TEM) using a Philips CM200 instrument. The microscope was equipped with a top-entry holder and ion pumping system, operating at an accelerating voltage of 200 kV and giving a nominal structural resolution of 0.21 nm. Samples were prepared by dipping a 3-mm holey carbon grid into ultrasonic dispersion of the oxide powder in ethanol

Photocatalytic runs (2 h) of phenol oxidation over the different catalysts (1 g/l) were performed in a Pyrex immersion well reactor (450 ml) using a metal halide 250 W lamp (Sylvania, metalarc HIS; exhibiting spectral lines above 390 nm, with main emission between 450–550 nm). In the oxidation tests, an oxygen flow was used to produce a homogenous suspension of the catalyst in the solution. Before each photo-experiment, the catalysts were settled in suspension with the reagent mixture for 15 min in the dark. The evolution of the initial phenol concentration (ca. 50 ppm in water) was followed by UV–vis spectrometry through the evolution of its characteristic 270 nm band, using a filtered aliquot ca. 2 ml of the suspension (Millipore Millex25 0.45-μm membrane filter). The degradation rates were calculated from the slopes of the conversion plots at the first 15 min of reaction, and assuming linear time dependence. The regression coefficients for such fittings are in all cases higher than 0.998.

3. Results and discussion

Under the experimental conditions of the study, the photodegradation of phenol displays a linear time dependence, with rate constants presented in Fig. 1. A linear time dependence is char-

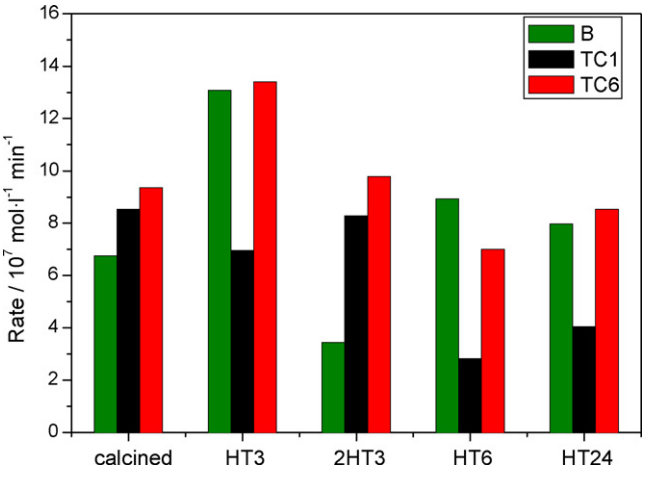

Fig. 1. Phenol photo-degradation reaction rate.

acteristic of phenol degradation at low concentrations [17–19]. Regarding to non-hydrotreated samples, comparison with the blank reference (series B) shows that anion doping on the solids (TC1 and TC6) may have a general positive, though moderate impact on photo-activity. This positive effect due to the presence of Cl/N seems to be higher as the Ti:Cl ratio increases. With respect to hydrotreated series, it can be observed that, in general, long treatment periods tend to diminish the photocatalytic activity. The maximum reaction rates are obtained for the samples hydrothermally pretreated for 3 h (Fig. 1), while larger periods of pre-treatment time are always pernicious for the reaction rate. Particularly, TC1 series displays a discrete evolution with no clear maximum value with (TC1) and HT3 (TC1-HT3) samples showing very similar reaction rates. Thus, from these results it can be assessed that the TC6-HT3 sample presents the best reaction rate, although the improvement with respect to the corresponding "only" calcined blank (B-HT3) reference sample is modest. For the TC1 series only the calcined and the TC1-2HT3 samples improve the corresponding result of the B series sample. Taking into account the specific experimental conditions and extrapolating these to reported photoactivities for phenol degradation [20], our best results in visible conditions clearly overcomes the corresponding value for commercial Degussa P25 (ca. 60% improvement) and appears similar to the UV highly photoactive TiO_2 materials.

XRD patterns of the samples are displayed in Fig. 2. All samples showing the characteristic pattern of anatase-TiO_2 (JCPDS 84-1286) without detection of any other contribution. The primary particle size obtained using the Scherrer equation is presented in Table 1. This table also includes the BET surface area. The reference ("only" calcined; without hydrotreatment) samples for each series (B, TC1 and TC6) show relatively high BET values (105–110 m^2/g) which appear independent of the Ti:Cl ratio used in their synthesis. The initial, 3 h of hydrotreatment moderately increases (decreases) surface area (primary particle size). On the other hand, large hydrotreatment periods, either in a continuous way or as a second HT3 treatment, lead to a general increase of the primary particle size and concomitant decrease of surface area. Such changes are in agreement with previous reports concerning the effect of the calcination/hydrotreatment steps on N-doped TiO_2-based morphological properties but here seem of modest magnitude [21,22]. We may mention here that only in the case of a 24-h hydrotreatment we detected the formation of the anatase phase prior to calcination. Within these hydrotreated samples, for B series it is observed a relative increase of the surface area as treatment time increases. TC1 and TC6 series present a similar trend, which differs from that

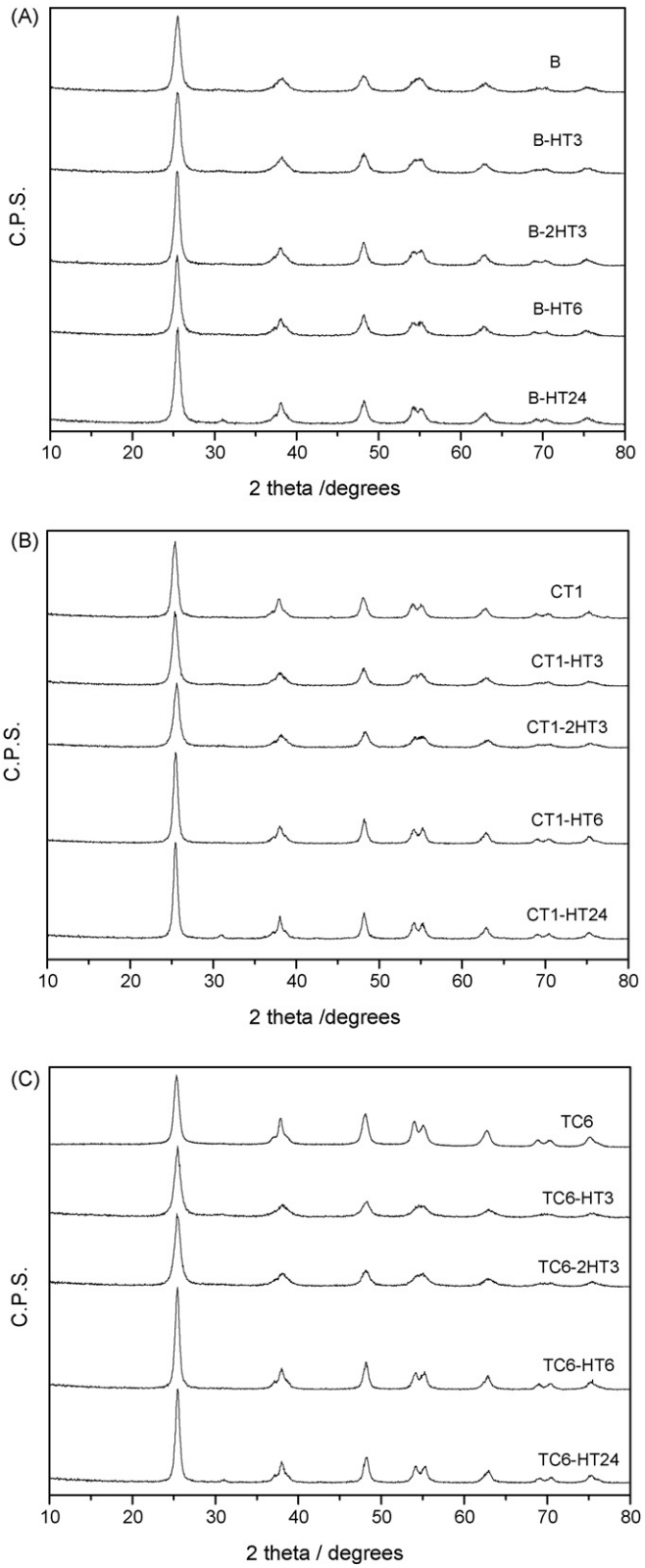

Fig. 2. XRD patterns of samples: (A) B; (B) TC1; and (C) TC6 series of samples.

of the B series and shows a maximum for the surface area after 3 (TC1) or 2 × 3 (TC6) h of hydrothermal treatment.

The pore size distribution of selected samples is shown in Fig. 3. For the reference ("only" calcined) samples, it is evident the effect of HCl and ammonia in the preparation method. Thus, as the Ti:Cl

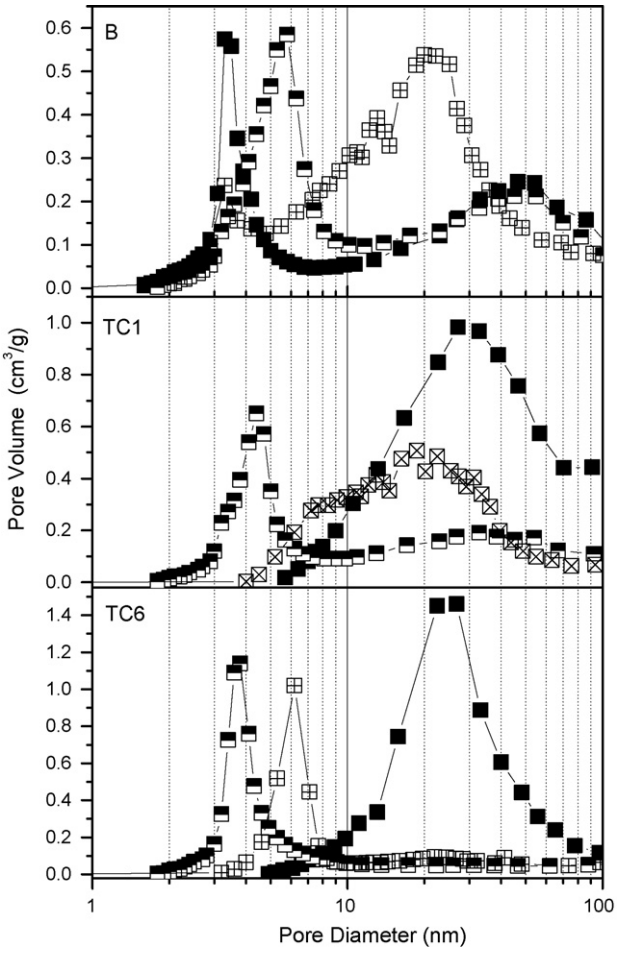

Fig. 3. Pore size distribution of the calcined (filled square), HT3 (half-filled square) and HT24 (crossed square) samples.

ratio increases we observed a significant shift of the mean pore size from ca. 5 nm for blank sample B to ca. 20–30 nm showed by the TC6 sample. The calcined B sample pore size distribution is clearly bimodal. It might be expected that the formation of a N, Cl-containing precursor induces a drastic change in the pore sizes (see below). The hydrotreatment also produces important modifications regarding the pore size distribution within the different series. Thus, for B series hydrotreatment produces the increase of the pore size, though long period seems to affect in a deeper way. On the contrary, for series TC1 and TC6 a short-time hydrotreatment leads to a significant decrease in the mean pore size. In these two series, large hydrotreatment times seem to modulate the pore size with respect to the corresponding B sample and then, after the overall 24 h of hydrotreatment, all (hydrotreated) TC6 samples exhibit moderate variations among them while the TC1 series display an intermediate behavior between the other two (B, TC6) set of samples. Consequently, the starting precursor (either an oxo-hydroxide for the B series or N, Cl-containing solids for TC1 and TC6 series) notably condition the evolution of the pore situation for short hydrotreatments, while large treatments develop closer pore structures, with a continuous change in going from B → TC1 → TC6.

The morphological characteristic of samples after this "extended" hydrotreatment step are also included in Table 1 for completeness. From Table 1 we only detected minor differences among the B and TC1/TC6 series of samples, varying the morphological properties of the samples in a similar way through all the series. This indicates that morphological properties summarized in Table 1 are mainly derived by the specific treatment to which the sample is subjected. The precursor nature and characteristics would thus seem of relatively less importance to control the titania polymorph and some (BET area, primary particle size) morphological characteristics of the samples. Other morphological properties related to the secondary particle size and porosity are however strongly dependent of the precursor nature. Fig. 4 provides visual information concerning the morphological features of B and TC6 selected samples. From these selected SEM images of the reference samples a clear different morphology can be inferred. Thus, B sample shows aggregates formed by small and homogeneous rounded particles of about 2–5 μm. On the other hand, TC6 appears developing heterogeneous aggregates having a larger variety of sizes and shapes. Therefore, the preparation of TiO_2 from an N, Cl-containing precursor clearly leads to a more heterogeneous morphology. This morphological difference could be in agreement with or drive to the pore size distribution presented in Fig. 2. Indeed, the existence of a wide pore size distribution and with a large fraction of pores having a high characteristic size is evident in the TC1/TC6 calcined samples if compared with the B material. The effect of hydrothermal treatment before calcination produces certain aggregation of the particles (Fig. 5) being more considerable for the B sample. As mentioned before, the long hydrotreatment period induces a modulation in the pore structure. From SEM images it can be notice that similar aggregated particles

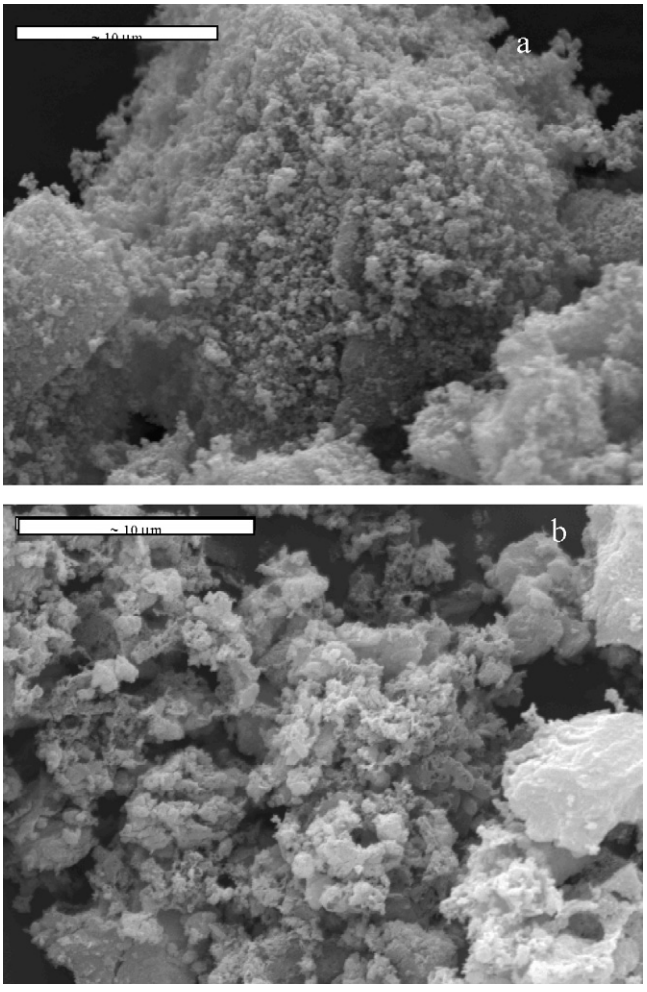

Fig. 4. SEM images for calcined (a) B and (b) TC6 samples.

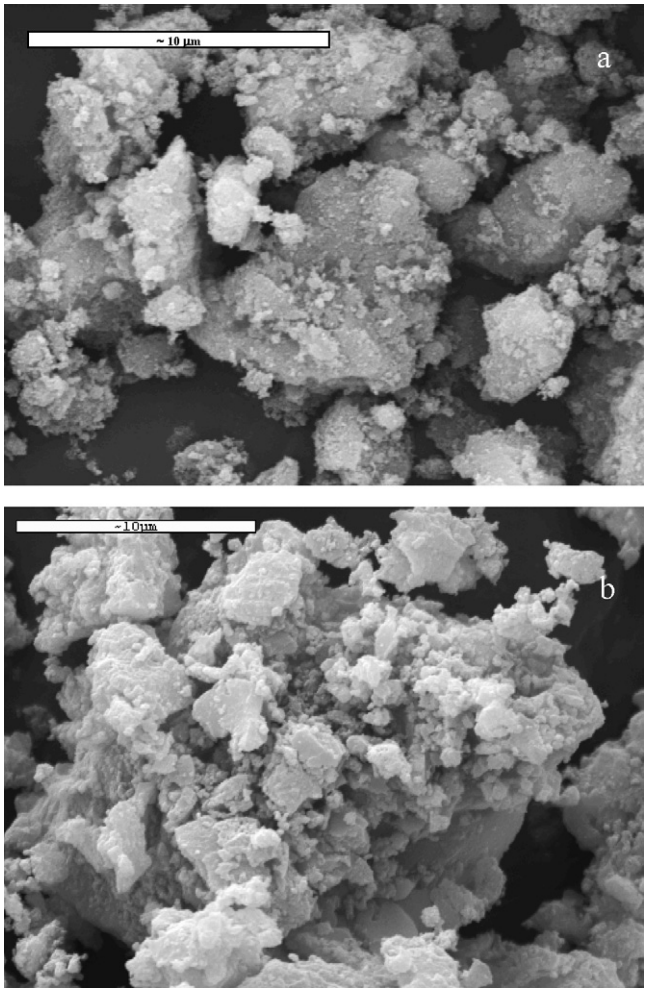

Fig. 5. SEM images for (a) B and (b) TC6 samples after 24 h of hydrothermal treatment and further calcined.

are found for B and TC6 samples though TC6 still show more heterogeneous shaped particles. This aggregation effect induced by the hydrothermal treatment is noticed in the selected TEM images shown in Fig. 6.

As well known, the photo-activity of anion-doped TiO_2-anatase samples under visible-light excitation is customarily related to physico-chemical phenomena associated with the presence of anion-related defects [3,5,6,8,10,11,13–16]. In order to clarify the N- and Cl-containing species present in our samples we combine results from XEDS, XPS, and DRIFTS. XEDS was unable to detect N and, more importantly, Cl in any of the samples (result not shown). Thus, according to chemical analyses, it might be eventually assumed a low loading of Cl species which was rather uniform, being in any case well below 0.4–0.3% for all samples. As halides species can be typically at the surface [10,11], the final calcinations step ensures the removal of mostly all surface species while a modest quantity seems to remain at the bulk in substitutional and/or interstitial positions. Fig. 7 shows a broad and featureless XPS peak at ca. 400 eV for all samples expect the blank, with a tail extending to lower binding energies which appear more markedly in the samples of the TC1 series. The main contribution at ca. 400 eV is customarily assigned to N—N, N—C, and N—O species, while the second (ca. 399 eV) is characteristic of neutral "NO" or N-containing species located in substitutional positions of the anatase network [23–25]. XPS also proves the absence of N^{3-} species in substitutional positions (binding energy ca. 396 eV) and the complete lack of Cl-containing species at the surface of the materials. The N-containing species nature will be further detailed with the help of IR. Fig. 8 displays the DRIFT spectra of the samples in the 2300–1900 cm^{-1} region. Three different contributions at ca. 2220–2210, 2150 and 2050 are clearly visible. Bands at ca. 2200 and 2150 cm^{-1} can be ascribed to stretching vibration of isocyanate $(CNO)^{n-}$ (the upper band) or, more likely, to cyanide $(CN)^{n-}$ species, both bands differing in the ionic degree/charge of the C—N bond by effect of the neighboring ions [15,26]. The assignment of the 2150 cm^{-1} is subjected to some doubts as may be also ascribed to NO^+ species [15,27], although the frequency is a little higher for such species in a titania matrix. Presence of NO^+ species is in any case confirmed by the 2050 cm^{-1} peak [15,27]. The presence of these N-containing species has been also observed by others using IR in N-doped TiO_2-based samples [15,28]. The three bands are present in the B/TC1/TC6 series of samples but behaving very differently as a function of the treatment mentioned in Table 1. As can be expected, sample B showed the less intense bands. The TC1 series displays mostly NO^+ species with a significant intensity for the "only" calcined sample followed by the TC1-2HT3 one. In the case of the TC6 series of samples, we unequivocally detect

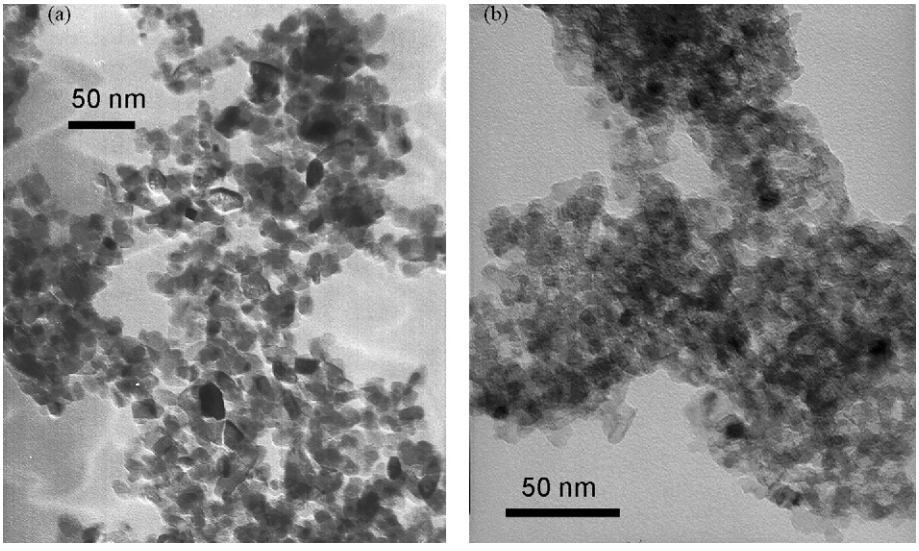

Fig. 6. TEM images for TC6 samples: (a) calcined and (b) after 3 h of hydrothermal treatment and further calcined.

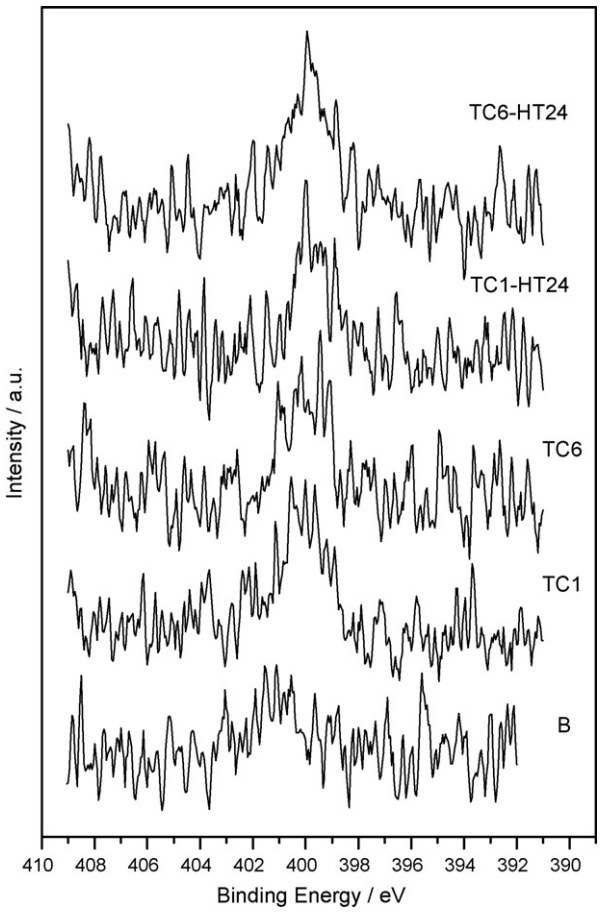

Fig. 7. N 1S XP spectra of selected samples.

the presence of both $(CN)^{n-}$ and NO^+ species with a maximum intensity for the TC6-2HT3 sample. A tentative correlation between the species observed with XPS and DRIFTS indicates that positively charged NO^+ species may be responsible for the 400 eV [23,24]. This type of species is, according to theoretical investigations, located in interstitial positions [14]. Negatively charged species, like $(CN)^{n-}$ species, could be occupying substitutional positions and are likely responsible for the tail peak at lower binding energy [23,24]. The presence of Ti–Cl bonds can be also analyzed with IR but, unfortunately, the corresponding bands are below 900 cm^{-1} and shadowed by the titania network contributions [29].

In spite of the somewhat limited chemical information obtained for anion impurities, a direct and very useful relationship can be established between the overall XPS/IR intensities of N-containing species and the UV–vis characteristics in the visible region (400–450 nm) displayed in Fig. 8. The UV–vis diffuse reflectance spectra show a localized band in such region for all samples expect the B reference, as previously observed by many others [3,5,10,11,15]. Obviously, the visible-light absorption power is a parameter of relevance in this context. Concerning the B series of samples, we see that the maximum visible-light absorption power corresponds to the B-2HT3 and B-HT6 samples. The ("only" calcined) TC1 sample is the one having higher visible-light absorption power (Fig. 9b) and IR intensity (Fig. 8b), followed by the TC1-HT6 and TC1-2HT3 samples in the decreasing, parallel behavior of both observables. For the TC6 series of samples, the calcined sample does not have a high N-derived impurity level and, consequently, a high visible-light absorption power; in this series, both observables are maximized for samples TC6-2HT3 and TC6-HT24. The close relationship of the UV–vis feature peaking at ca. 425–450 nm and the N-content of the sample measured by XPS/DRIFTS seems thus of general validity within our preparation procedure. In contrast, the analysis of the bandgap of the TiO_2-anatase presented in Table 2 indicates a constant value within experimental error (ca.

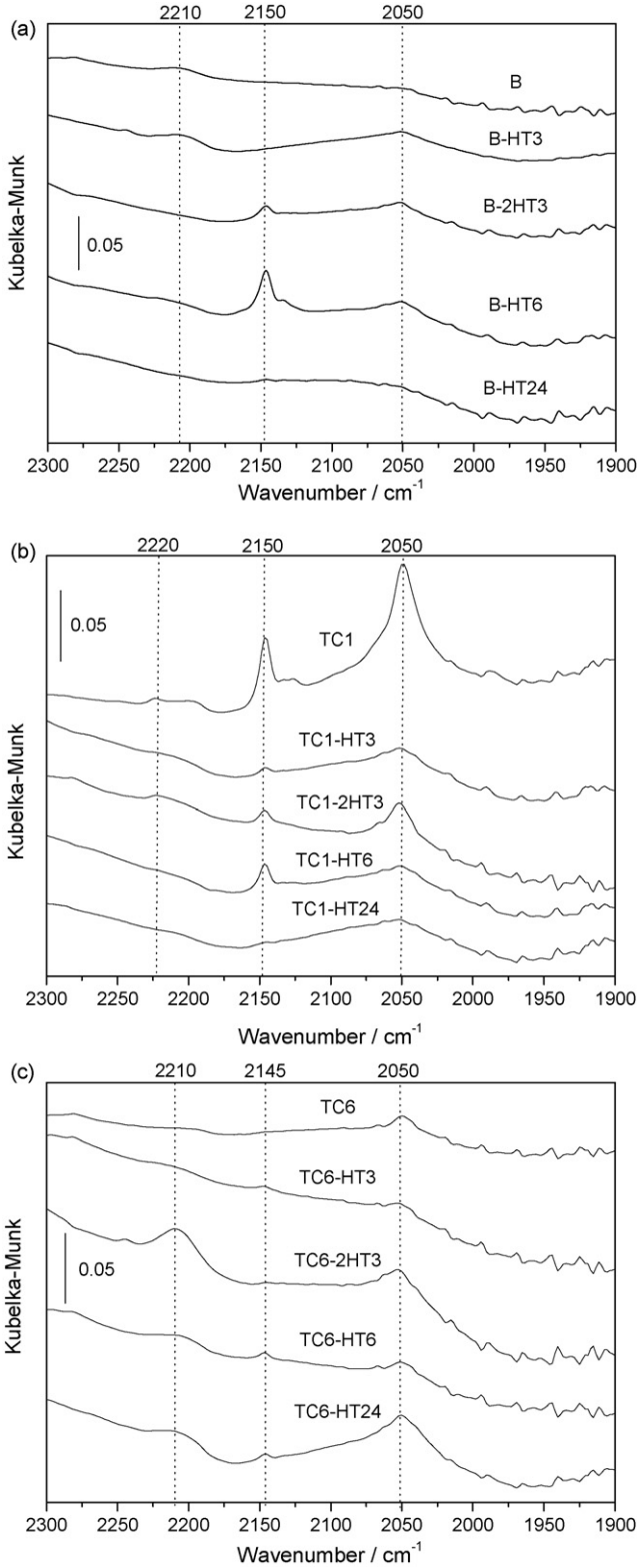

Fig. 8. DRIFT spectra of (a) B, (b) TC1 and (c) TC6 series of samples.

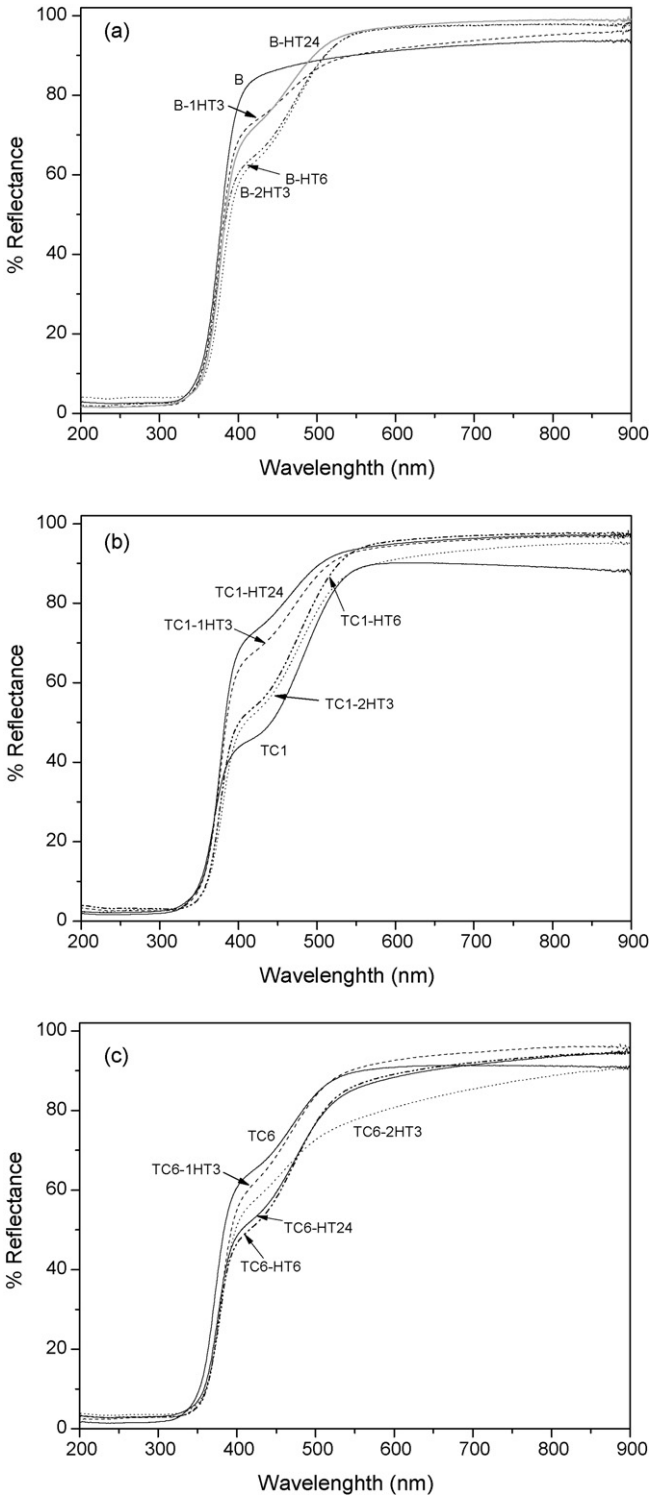

Fig. 9. UV–vis spectra of samples: (a) B; (b) TC1; and (c) TC6 series of samples.

0.2 eV), irrespective of considering the solid as an indirect (like the microsized anatase) or direct (by an effect of the particle size) semiconductor [30]. This is in agreement with previous literature reports which showed the absence of major changes in the valence and conduction bands of the anatase material and the presence of N-derived localized states near the valence band top [3,5,6,8,13–15]. Additionally, no halide-derive band modification of the conduction is visible [12], presumably by its low concentration.

From the direct link between the N-content of the samples and the visible-light absorption power we can extract two main consequences. First is the obvious point that such a UV–vis band is not associated with any specific N-containing species. In fact, previous theoretical studies were able to show that both species may drive to the same light absorption feature (at least when the UV–vis absorption peak is as broad as can be seen in Fig. 5) irrespective of the specific chemical nature of the species (see Refs. [13,14] and references therein). The pale yellow color of the samples is therefore indicative of the N-content, being essentially insensitive to the chemical nature of the N species in our case. The second consequence concerns the photo-catalytic activity behavior. Comparison with Fig. 1 indicates that the visible-light absorption power or, alternatively, the N-content of the materials is not correlated with the reaction rate. For each specific treatment, e.g. each column of Fig. 1, the maximum rate is observed for the corresponding TC6 samples in most of the cases. On the other hand, the reaction rates behaves very similarly in the three series of samples (including the B reference samples) with the treatment suffered by the solid precursor, indicating that morphological aspects are of importance in qualitatively explaining photo-activity under visible-light excitation. On the other hand, the primacy of the TC6 series may be likely derived from the presence of an specific negatively charged N-containing species, possibly $(CN)^{n-}$. We may speculate that the higher initial Cl concentration of the precursor may favor the presence of this species. This hypothesis needs further investigation. Obviously, the photochemical relevance of such $(CN)^{n-}$ species would not be related to a different or characteristic visible-light absorption power but more likely to a certain influence in the recombination of charge carriers. The modulation of the photo-activity through each sample series (row in Fig. 1) seems however less important than the increase of the reaction rate detected for the corresponding TC6 sample for each column of Fig. 1. This would suggest that, firstly the presence of $(CN)^{n-}$ species (which could participate in the photocatalytic mechanism), and secondly and possibly less importantly, the adequate surface and morphological features are key points to maximize activity. In particular, the notable increment on surface area (Table 1) and the adequate pore size distribution (Fig. 2) appear to play critical roles and are likely the morphological key properties. Therefore, we can conclude that the presence of N species and its related absorption band in the visible do not grant the finest performance in the catalyst for a photocatalytic application. As a result join, surface, pore distribution and structural contributions lead to better photoactivity rates for phenol degradation by improving the overall photocatalytic mechanism [20].

Table 2
TiO_2-anatase bandgap energies

Sample	Bandgap (eV)	
	Direct	Indirect
B	3.37	3.11
B-HT3	3.36	3.09
B-2HT3	3.25	2.94
B-HT6	3.32	2.99
B-HT24	3.30	3.04
TC1	3.36	2.88
TC1-HT3	3.31	3.04
TC1-2H3	3.24	2.95
TC1-HT6	3.28	2.96
TC1-HT24	3.28	3.05
TC6	3.33	3.01
TC6-HT3	3.26	3.01
TC6-2HT3	3.24	3.10
TC6-HT6	3.26	3.06
TC6-HT24	3.26	3.05

4. Conclusions

It has been shown that the hydrotreatment is an optimum procedure to control the surface and morphological aspects of the studied photocatalysts. Samples hydrotreated for 3 h present the best photocatalytic performance. These activity maxima could be related with the maximization of the surface area as well as the existence of an adequate pore size distribution. In addition, the presence of certain negatively charged nitrogenated species such as $(CN)^{n-}$, could also participate in a certain positive way, possibly related with the charge recombination step of the photocatalytic mechanism. It is also important to point out that the improvement of the photocatalytic activity could not be directly associated to the visible absorption power of anion-doped samples. On the basis of these considerations, the best series correspond to TC6 samples, being the optimum value the sample hydrotreated for 3 h and further calcined. This sample would present a synergic situation in which surface, pore distribution and anion-doped-related structural aspects contribute positively to the reaction rate.

Acknowledgements

Financial support by the projects CTQ2004-05734-CO2-02, CTQ-2007-60480/BQU, and P06-FQM-1406 is fully acknowledged. P.S. thanks the Spanish Ministerio de Educación y Ciencia for a predoctoral FPI fellowship.

References

[1] N. Serpone, E. Pelizzetti (Eds.), Photocatalysis Fundamental and Applications, Wiley, New York, 1989.
[2] M.R. Hoffmann, S.T. Martin, W. Choi, D.W. Bahnemann, Chem. Rev. 95 (1995) 69.
[3] G. Colón, C. Belver, M. Fernández-García, Photocatalysis, in: M. Fernández-García, J.A. Rodríguez (Eds.), Synthesis, Properties and Application of Oxide Nanoparticles, Wiley, USA, 2007 (Chapter 17).
[4] H. Thu, M. Karkmaz, E. Puzenat, C. Guillard, J.M. Herrmann, Res. Chem. Intermed. 31 (2005) 449.
[5] J. Zhao, C. Chen, W. Ma, Topics Catal. 35 (2005) 267.
[6] D. Chatterjee, S. Dagupta, J. Photochem. Photobiol. C 6 (2005) 186.
[7] R. Asahi, T. Morikawa, T. Ohwaki, K. Aoki, Y. Ega, Science 293 (2001) 269.
[8] N. Serpone, J. Phys. Chem. B 110 (2006) 24287.
[9] T.L. Thompson, J.T. Yates, Chem. Rev. 106 (2006) 4428.
[10] D. Li, H. Haneda, S. Hishita, N. Ohashi, Mater. Sci. Eng. B 117 (2005) 67.
[11] D. Li, H. Haneda, S. Hishita, N. Ohashi, Chem. Mater. 17 (2005) 2596.
[12] M. Long, W. Cai, Z. Wang, G. Liu, Chem. Phys. Lett. 420 (2006) 71.
[13] A. Nambru, J. Graciani, J.A. Rodríguez, Q. Wu, E. Fujita, J. Fernández-Sanz, J. Chem. Phys. 125 (2006) 094706.
[14] E. Finazzi, C. Di Valentin, A. Selloni, G. Pacchioni, J. Phys. Chem. C 111 (2007) 9275.
[15] C. Belver, R. Bellod, S.J. Steward, F.G. Requejo, M. Fernández-García, Appl. Catal. B: Environ. 65 (2006) 309.
[16] S.J. Steward, M. Fernández-García, C. Belver, B.S. Mun, F.G. Requejo, J. Phys. Chem. B 110 (2006) 16482.
[17] G. Colón, M.C. Hidalgo, J.A. Navío, Appl. Catal. B 45 (2003) 39.
[18] J. Medina-Valtierra, E. Moctezuma, M. Sánchez-Cárdenas, C. Fraustro-Reyes, J. Photochem. Photobiol. A 174 (2005) 246.
[19] G. Colón, M.C. Hidalgo, G. Munuera, I. Ferino, M.G. Cutrufello, J.A. Navío, Appl. Catal. B 63 (2006) 45.
[20] G. Colón, M.C. Hidalgo, J.A. Navío, E. Pulido Melián, O. González Díáz, J.M. Doña, Appl. Catal. B: Environ. 78 (2008) 176.
[21] S. Yin, Y. Aita, J. Wang, Q. Tang, T. Sato, J. Mater. Chem. 15 (2005) 674.
[22] T.-Y. Han, C.F. Wu, C.-T. Hsieh, J. Vac. Sci. Technol. B 25 (2007) 430.
[23] D. Li, H. Huang, X. Chen, Z. Chen, W. Li, D. Ye, X. Fu, J. Solid State Chem. 180 (2007) 2630.
[24] C. Chen, H. Bai, C. Chuang, J. Phys. Chem. C 111 (2007) 15228.
[25] T. Morikawa, R. Asahi, Chem. Phys. 339 (2007) 57.
[26] Z. Wang, U. Helmersson, P.O. Kall, Thin Solid Films 405 (2002) 50.
[27] K.I. Hadjiivanov, Catal. Rev. 42 (2000) 71.
[28] C. Li, L. Chen, N.M. Dimitrijevic, K.A. Gray, Chem. Phys. Lett. 451 (2008) 75.
[29] R.H. West, G.J.O. Beran, W.H. Green, M.K. Kraft, J. Phys. Chem. A 111 (2007) 3560.
[30] M. Fernández-García, A. Martínez-Arias, J.C. Hanson, J.A. Rodríguez, Chem. Rev. 104 (2004) 4063.